

## OPTIMIZATION OF A LOUVERED FIN HEAT EXCHANGER WITH INDIVIDUALLY VARIABLE LOUVER ANGLES

Ameel B. \*, Degroote J., Huisseune H., De Jaeger P. , Vierendeels J. and De Paepe M.

\*Author for correspondence

Department of Flow, heat and combustion mechanics

Ghent University,

Belgium

E-mail: Bernd.Ameel@Ugent.be

### ABSTRACT

In this study, a round tube and fin geometry with individually varying louver angles is analyzed. The thickness of the fin was neglected. Any interactions between the optimal louver angles and the fin thickness are hence not captured. A laminar and steady calculation was performed, with symmetric boundary conditions. For the Reynolds number on the hydraulic diameter ( $Re_{Dh}$ ) of 535 that was studied, a Von Karman vortex street is present behind the last tube row of heat exchanger. The steady calculation is hence only an approximation of the reality, but is shown to give reasonable results. An ordinary kriging response surface model was used to explore the entire parameter space. Updates to the model were made on the basis of improving the Pareto front, visualizing the tradeoff between heat transfer and pressure drop. It is shown that the use of individually varying louver angles allows increasing the Colburn  $j$  factor by 1.3% for the same friction factor, with respect to the optimal uniform louvered fin configuration.

### INTRODUCTION

Louvered fin and tube heat exchangers are often used in HVAC systems. Many researchers have studied the louvered fin, either with flat tubes [1-3] or with round tubes [4-6]. Both experimental and numerical work has been done. In most of these studies, a single louver angle is used for all the louvers. Jang and Tsai [7] investigated the optimum uniform louver angle for a flat tube and louver heat exchanger. Hsieh and Jang [8] considered a variable louver angle, where the louver angle successively increases or decreases. This research was also done for a flat tube configuration. Leu et al. [5] studied the influence of the louver angle on a louvered heat exchanger with round or oval tubes, with constant louver angle. They neglected the fin-louver junction, modelling rectangular louver shapes without transitions. As already indicated by Tafti and Cui [9],

strong three-dimensionality is present in the transition zones connecting the louver to a flat tube. It is reasonable to assume that the transition zones connecting the louver to the fin in a round fin and tube heat exchanger will also exhibit strong three-dimensional behaviour. Therefore the transition zones are modelled in this work. An X-shaped configuration with transition zones is assumed for the louvers. This allows taking the three-dimensionality of the louver shape itself and of the transition zones into account. Regrettably, this required neglecting the fin thickness effect for the flow domain.

In this paper, the optimal louver angle for a round fin and louver configuration will be studied, while taking all three-dimensional effects of louver shape and transitions into account. The louver angles in front of the turnaround louver are individually variable. The louver configuration is symmetrical around the turnaround louver.

### NOMENCLATURE

$j$	[-]	Colburn $j$ factor
$f$	[-]	Friction coefficient as defined in Wang [6]
$Q$	[W]	Heat transfer
$P$	[Pa]	Pressure drop
$Re_{Dh}$	[-]	Reynolds number on frontal speed and hydraulic diameter of the fin channel
$Re_{Do}$	[-]	Reynolds number on frontal speed and tube outer diameter
$p$	[-]	Observed order of convergence of the numerical scheme
<i>Subscripts</i>		
$ref$		reference, all louver angles equal to 15°
$0$		

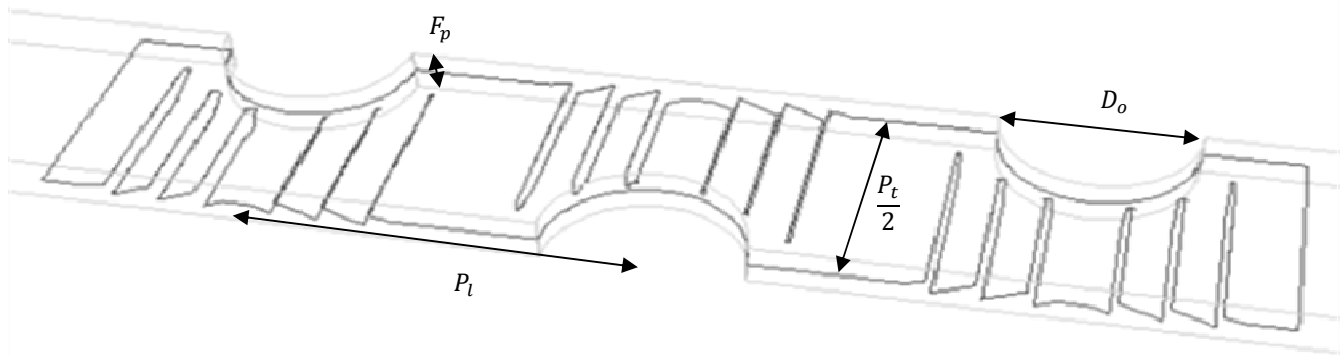


**Figure 1 Heat exchanger geometry**

### GEOMETRY AND BOUNDARY CONDITIONS

The geometry of the computational domain is shown in Figure 1. The studied geometry consists of 3 tube rows in a staggered layout, with louvered fins around each tube. Half of a periodic unit cell is modeled, with the side planes having symmetric boundary conditions. This is allowed because the Von Karman vortex street is not modeled in the steady state simulation. The top and bottom planes are periodic. The inlet of the numerical domain is 2 tube diameters ahead of the heat exchanger and 20 tube diameters behind the heat exchanger. These regions are not shown in Figure 1. The inlet condition is a uniform velocity profile at 2.69 m/s, the outlet condition is a uniform constant pressure condition. The inlet and exit regions allow taking the entrance and exit effects of the heat exchanger into account. The tube walls are at a constant temperature of 323.15 K, the inlet temperature is 293.15 K. The fin material has zero thickness for the flow domain, for the material domain the thickness is 0.12 mm. The conductivity is equal to 202.4 W/mK, corresponding to an aluminum alloy. There is one inlet louver, 2 regular louvers, a turnaround louver, another two regular louvers and the outlet louver. The inlet louver, the two regular louvers and the turnaround louver can all have different angles. The other louver angles are determined from the symmetry condition.

Other geometrical parameters are summarized in Table 1. Figure 2 shows the louver geometry itself and the dimensions of the X-shaped louver.

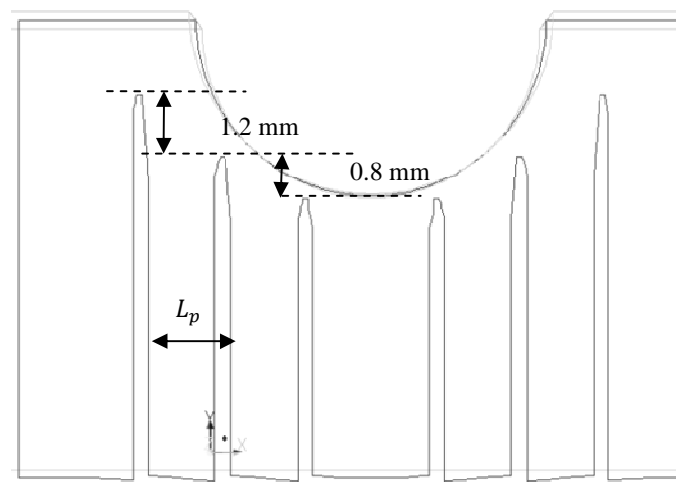


**Figure 2 Louver geometry**

### NUMERICAL METHOD

The numerical simulation was done with the commercial software Fluent. In order to be able to mesh the louver-fin transition adequately, a zero fin thickness model is used. The heat transfer in the fin material is modelled used the conduction equations in a single layer of cells conforming to the geometry of the fin. This allows taking fin efficiency effects into account. As was done in the study of Leu et al. [5], the flow is assumed to be three dimensional, laminar and steady. This is a great simplification of reality. For the frontal speed considered in this research (2.69 m/s), the Reynolds number on the outer tube diameter ( $Re_{D_o}$ ) is 1158. For this value, a Von Karman vortex street would be present around a tube in free stream. This vortex is suppressed due to the presence of the fins in the interior of the heat exchanger. However, behind the last tube row no further obstacles to the flow are present. The length of the fin behind the tube is small compared to the expected tube wake. The flow behind this tube row is hence physically unsteady. A single unsteady simulation was performed for a flat fin. Unsteadiness occurs behind the last tube, causing small fluctuations in overall pressure drop and heat transfer around a mean value. These fluctuations are only 0.1% of the mean

**Table 1 Geometrical parameters**

Fin pitch	$F_p$	1.71 mm
Transversal tube pitch	$P_t$	17.6 mm
Longitudinal tube pitch	$P_l$	13.6 mm
Fin thickness (for material)	$t_f$	0.12 mm
Louver angles	$\theta$	15° to 35°
Louver pitch	$L_p$	1.5 mm
Tube outer diameter	$D_o$	6.75mm

value for heat transfer and even less for the pressure drop. In the steady laminar simulation, there is no mixing of the high velocity fluid from contract area in the last tube row with the surrounding fluid. In an unsteady simulation, there is mixing due to the unsteady eddies. Therefore, a viscosity profile was imposed behind the heat exchanger to simulate this mixing. Without this mixing, the jet of fast fluid due to the accelerated flow between the tubes of the final tube row persists up to the exit boundary. The viscosity profile has negligible influence on the flow inside the heat exchanger and ensures well mixed flow at the outlet of the numerical domain. This is necessary to capture the pressure recovery at the heat exchanger exit due to expansion of the flow when leaving the heat exchanger core. With this measure, the difference between the steady simulation and the average of the unsteady simulation was less than 0.2% for heat transfer and pressure drop. This indicates that results made by this approximation will be reasonable, even though they do not correspond to a physical solution.

### Accuracy of the numerical simulations

The discretization schemes are second order upwind for pressure, momentum and energy. The grid convergence was checked with Roache's grid convergence index [10]. A Taylor expansion of a quantity of interest is made in function of the grid cell size, around the limiting case of zero cell size. In this case, the heat transfer rate  $Q$  is used.

$$Q_h - Q_0 = \left. \frac{\partial Q}{\partial h} \right|_0 h^p + O(h^{p+1}) \quad (1)$$

If all calculations are in the asymptotic range, the higher order terms can be neglected. This results in an equation with 3 unknowns,  $Q_0$ ,  $\left. \frac{\partial Q}{\partial h} \right|_0$  and  $p$ . Three simulations for three different grid sizes are entered into this equation. Here it is assumed that the same expansion is valid for all three equations. This is only valid for geometrically similar meshes. This condition is not met for unstructured grids. Both the mesh shape and mesh size change between the different calculations. As such this equation is mathematically not fully valid, but it is a good approximation as long as the errors due to grid shape are similar for all meshes considered. The grid size  $h$  is derived from the total number of cells, by  $h = C \cdot \sqrt[3]{N}$  with  $C$  an arbitrary constant. It was chosen so that the grid size matches the average cell size on the coarsest grid.

The finest grid had an average cell size of 0.08 mm. The average cell size on the coarsest grid is 0.13 mm.

With these three grids, the values for  $Q_0$ ,  $\left. \frac{\partial Q}{\partial h} \right|_0$  and  $p$  are determined. If the observed order of convergence  $p$  matches the theoretical order of convergence of the discretization scheme, the calculations can be assumed to lie in the asymptotic range. The difference between  $Q$  on a grid and  $Q_0$  gives an estimate for the discretization error, which is 0.5% for the heat transfer and 2.3% for the pressure drop on the coarsest grid. The observed order of convergence for the heat transfer is 1.80, for the pressure drop this is 3.06. The difference between the pressure drops on both grids is only 0.5%, the large estimate for the error is because the asymptotic rate of convergence is not yet reached for all three grids. This means that the  $O(h^{p+1})$

term in the equation is not negligible. According to Roache [10], a factor of safety of 3 is required to correct the error estimate if the observed order of convergence differs by more than 10%. The coarsest grid consists of around 4 million cells. The finest grid contains 26 million cells. In order to have reasonable computation times, the coarsest grid was used for the other calculations.

The resulting  $j$  and  $f$  values were also compared with the Wang correlation for louvered fin and tube heat exchangers [6], with the thickness equal to the virtual thickness used to calculate the material domain. The error on the Colburn  $j$  factor is 5%, the error on the friction factor is 12.1%. The Wang correlation has a deviation of  $\pm 15\%$  for 90.8% of all data used to fit the correlation. These results are hence acceptable.

It is however important to note that fin thickness effects are not taken into account. This fin thickness decreases the minimum flow area and hence increases the local velocities and thus the pressure drop and heat transfer. This effect is however similar for all geometries studied, and should therefore not strongly influence the optimal louver geometry.

### RESPONSE SURFACE MODEL

In total there are 4 parameters which dictate the shape of the louvers. There are 8 angles in total (inlet, outlet, 4 regular louvers, 2 parts of the turnaround louver). As symmetry with respect to the turnaround louver is imposed, there are 4 remaining parameters. Each tube row has the same louver geometry. As every calculation takes around 4 hours, it is important to only calculate interesting designs. This requires predicting the value of the heat transfer and pressure drop at unknown designs. For that reason, a response surface model (RSM) is fitted to the data. Specifically, an ordinary kriging response surface model is used. This is an interpolating RSM which gives a prediction and an estimate for the error [11]. In every possible point, there is an estimate of the probability distribution of the value which will be obtained if the design would be calculated. This error estimate allows making the trade-off between well explored areas and unexplored areas, by considering the expected improvement by actually calculating the design.

For the initial sampling of the data when there is no prior knowledge whatsoever, latin hypercube sampling (LHS) is used. This is a sampling plan which has good space-filling properties. The sampling plan is stratified in every variable, which means that the projection of the plan on every axis will not result in overlapping points. For the LHS used in this paper, the projection results in equidistantly spaced points. A second property of an optimal LHS is that the minimal distance between all points in the sampling plan, is as large as possible. This is the minimax criterion. The LHS is generated heuristically, so the minimax criterion is only approximated.

An initial 10 designs are sampled according to the LHS sampling plan, and a kriging RSM is fitted to the data. Two separate kriging models are used, one for the pressure drop and one for the heat transfer. All data is normalized with the pressure drop and heat transfer of the reference design, which is the uniform louver angle at  $15^\circ$ . At the locations where the

error is largest according to the RSM, new designs are calculated. At this point these error estimates are still highly unaccurate. The RSM is updated until the error estimates become reasonably constant as further data is added to the model.

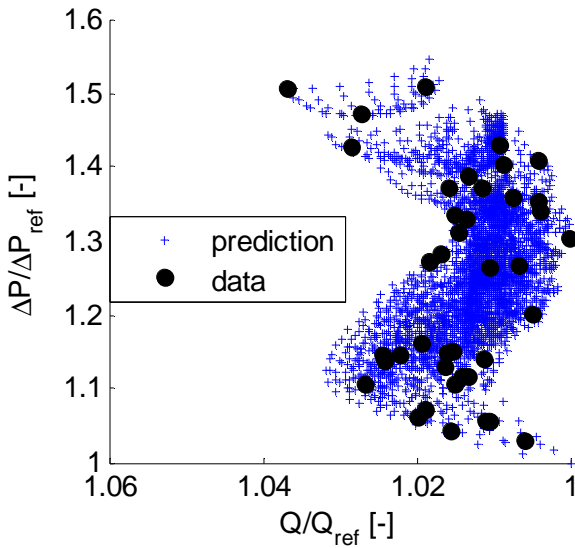


**Figure 3 Q-P diagram after 40 calculations**

The RSM is sampled fully factorial with 10 levels, and all values for the heat transfer and pressure drop are shown on Figure 3. For any single heat transfer value, there are many possible designs, each with a different pressure drop. The design with the minimal pressure drop is always better than all the other designs with that heat transfer value. The combination of all designs which have the optimal trade-off between heat transfer and pressure drop is the Pareto front, which is sketched by the discontinuous line. This is an estimate of the Pareto front generated by the RSM. There is also the Pareto front formed by the actually calculated points. For each predicted point, the probability that this point will improve the Pareto front of the calculated designs can be determined. This is done by using numerical integration of the probability density function. This probability is then weighted by the distance in the Q-P plane to the nearest already calculated point, to estimate the amount the Pareto front is improved.

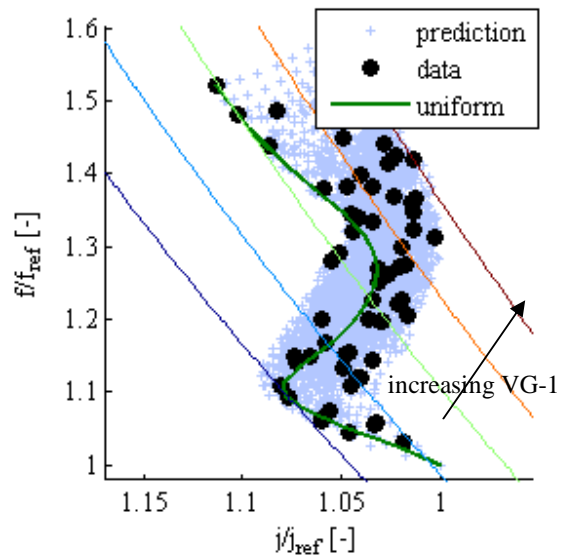


**Figure 4 Data in the j-f plane, with indication of VG-1 criterion, 61 calculations**

As more data is added to the RSM, based on the criterion that the weighted probability of improvement of the Pareto front must be maximal, more actual calculations lie on the predicted Pareto front. The data is reduced to the Colburn j factor and friction factor, and again all designs are displayed on Figure 4. To compare different designs on the Pareto front, contours of constant VG-1 variable geometry PEC by Webb [12] are also displayed. Between the extremes, the VG-1 PEC varies from 1.15 for the worst design, to 0.9 for the best design. A value of one corresponds to the value of the reference design, the constant louver angle of 15°. The VG-1 PEC indicates the reduction of total heat transfer area that can be obtained compared to the reference fin, under the constraints of same fan power, mass flow rate and heat transfer.

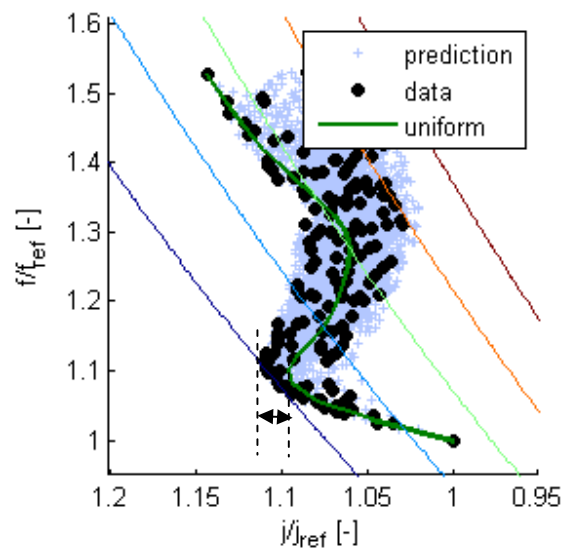


**Figure 5 j-f plane with indication of uniform louver angle designs, final update of the RSM, 164 calculations**

When more data is added, the shape of the prediction curve does not change very much. This indicates that the RSM is now able to predict the values quite well. On Figure 5, the final iteration of the RSM is represented. There are barely any predictions that still outperform the Pareto front determined by the calculations. It can also be seen that the uniformly louvered designs closely approach the Pareto front throughout the design space. There is only a small region indicated by the dashed lines, where the variable louver angles improve the performance over the uniformly louvered fin. In this region the Colburn j factor is improved by 1.3% for the same friction factor as the constant louver angle fin. This is a significant fraction of the total variation of 14% in Colburn j factor over the entire design space.

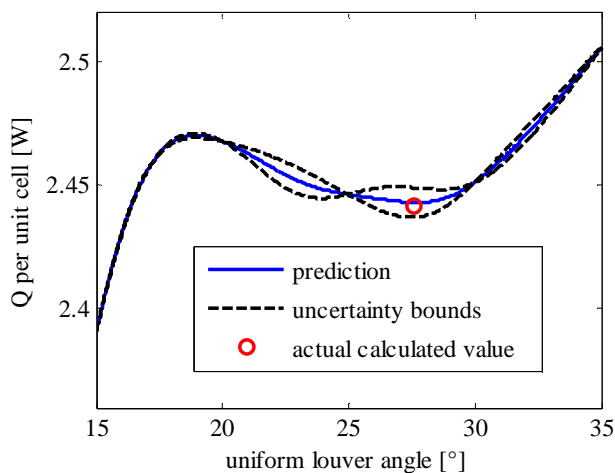


**Figure 6 Heat transfer in function of uniform louver angle**

On Figure 6 the RSM is explored for designs with constant louver angles. Both the prediction and the 95% confidence interval are shown. There are a few points where the confidence interval reaches zero width. This is because of the interpolating condition of the RSM. When a calculation is known in a point, the error in that point is estimated to be zero. For designs very similar to a calculated point, the error will still be small. How quickly the estimated error rises with increasing distance from data points is determined by the correlation length observed from the data. This is done for each dimension separately.

An interesting feature of the heat transfer is that it exhibits a local maximum and a local minimum. As the pressure drop increases monotonically with the louver angle (not shown), the region where the heat transfer drops in function of louver angle is not interesting. This can be seen on Figure 5 by observing the line representing the uniform designs. Starting from the point (1, 1) corresponding to the reference case of uniform louver angles of 15°, first the j and f factors increase, up until a certain point. Then the j factor decreases for increasing f factors, until the j factor starts to increase again and eventually is restored to the value before it started to decrease. From the start of the decrease to the recovery is the uninteresting zone where other designs can deliver the same heat transfer for lower pressure

drop. This is the region where the uniform louver line departs from the Pareto front.

This region is also the region in Figure 6 where the uncertainty is quite high, compared to the increasing parts of the function. The RSM detected that the probability of having a design on the Pareto front occurring in this region is very low and doesn't expect any improvement to the Pareto front by calculating points in this region. Very few calculations are hence requested in this region. Because of the lack of data, the uncertainty is relatively high. In order to illustrate the accuracy of the error estimate, a calculation was requested manually in the region of high uncertainty and low expected improvement. The actual result is a good match with the prediction and lies well within the uncertainty bounds.

From Figure 5 it is clear that the individually varying louver angles can offer a slight improvement in the surface area. The reason for this is that the Pareto front of the variable louver angles shows an increase of j with louver angle up to higher louver angles. This is accompanied by an increased friction factor. The point with the greatest Colburn j factor in the design space is the constant maximal louver angle design. Individually varying louver angles hence does not increase the maximal Colburn j factor.

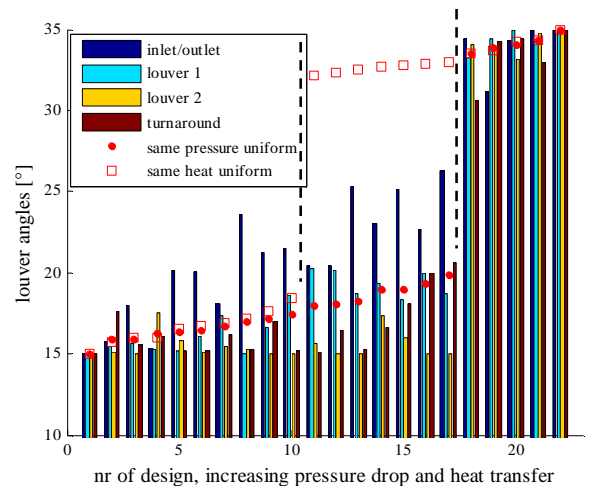


**Figure 7 Geometry of the designs and equivalent constant louver angle design**

Figure 7 shows the geometry of the different designs on the Pareto front. Every design is represented by 4 bars, whose heights indicate the louver angle. They are sorted by increasing heat transfer. For each design, the prediction for the heat exchanger with uniform louver angles that gives the same heat or pressure drop is also indicated.

For the range of low heat transfer rates, limited by the leftmost dashed line, there is very little difference between the two equivalent louver angles. This means that whether the variable louver angle geometry or constant louver angle geometry is used, the heat transfer and pressure drop is more or less the same. This is followed by a region in design space where there is a large difference between the louver angles of equivalent heat transfer and equivalent pressure drop. This is

the region where the variable louver angle geometry makes sense. The main feature of these designs is that the inlet and outlet louvers are at a higher angle than the other louvers. Finally, for even high heat transfer rates, there is again no more difference between the uniform louver angle designs and the variable louver angle designs. The Pareto fronts of uniform angles and of variable angles coincide again.

## CONCLUSION

Combining an ordinary kriging response surface model with CFD calculations allows focussing computational effort on interesting designs. Fin designs that are dominated by other designs that are better in any case are not explored. Using variable louver angles does not offer a significant advantage over a constant louver angle. The Colburn  $j$  factor is increased by only 1.3% for the same friction factor as the usual constant louver angle fin. As the total variation of  $j$  over the design space is only 14%, this improvement is not negligibly small.

## REFERENCES

- [1] C. Cuevas, D. Makaire, L. Dardenne, and P. Ngendakumana, "Thermo-hydraulic characterization of a louvered fin and flat tube heat exchanger," *Experimental Thermal and Fluid Science*, vol. 35, pp. 154-164, 2011.
- [2] V. P. Malapure, S. K. Mitra, and A. Bhattacharya, "Numerical investigation of fluid flow and heat transfer over louvered fins in compact heat exchanger," *International Journal of Thermal Sciences*, vol. 46, pp. 199-211, 2007.
- [3] J. Dong, J. Chen, Z. Chen, W. Zhang, and Y. Zhou, "Heat transfer and pressure drop correlations for the multi-louvered fin compact heat exchangers," *Energy Conversion and Management*, vol. 48, pp. 1506-1515, 2007.
- [4] H. Huisseune, C. T'Joel, P. De Jaeger, A. Willockx, and M. De Paepe, "Study of junction flows in louvered fin round tube heat exchangers using the dye injection technique," *Experimental Thermal and Fluid Science*, vol. 34, pp. 1253-1264, 2010.
- [5] J.-S. Leu, M.-S. Liu, J.-S. Liaw, and C.-C. Wang, "A numerical investigation of louvered fin-and-tube heat exchangers having circular and oval tube configurations," *International Journal of Heat and Mass Transfer*, vol. 44, pp. 4235-4243, 2001.
- [6] C. C. Wang, C. J. Lee, C. T. Chang, and S. P. Lin, "Heat transfer and friction correlation for compact louvered fin-and-tube heat exchangers," *International Journal of Heat and Mass Transfer*, vol. 42, pp. 1945-1956, 1998.
- [7] J.-Y. Jang and Y.-C. Tsai, "Optimum louver angle design for a louvered fin heat exchanger," *International Journal of the Physical Sciences*, vol. 6, pp. 6422 - 6438, 2011.
- [8] C.-T. Hsieh and J.-Y. Jang, "3-D thermal-hydraulic analysis for louver fin heat exchangers with variable louver angle," *Applied Thermal Engineering*, vol. 26, pp. 1629-1639, 2006.
- [9] D. K. Tafti and J. Cui, "Fin-tube junction effects on flow and heat transfer in flat tube multilouvered heat exchangers," *International Journal of Heat and Mass Transfer*, vol. 46, pp. 2027-2038, 2003.
- [10] P. J. Roache, "Perspective: A Method for Uniform Reporting of Grid Refinement Studies," *Journal of Fluids Engineering*, vol. 116, pp. 405-413, 1994.
- [11] A. I. J. Forrester and A. J. Keane, "Recent advances in surrogate-based optimization," *Progress in Aerospace Sciences*, vol. 45, pp. 50-79, 2009.
- [12] R. L. Webb, "Performance evaluation criteria for use of enhanced heat transfer surfaces in heat exchanger design," *International Journal of Heat and Mass Transfer*, vol. 24, pp. 715-726, 1981.